Applied Surface Science 532 (2020) 147461

Contents lists available at ScienceDirect

Applied Surface Science

journal homepage: www.elsevier.com/locate/apsusc

Defect engineering on MoS_2 surface with argon ion bombardments and thermal annealing

Weigang Lu, Blake Birmingham, Zhenrong Zhang*

Department of Physics, Baylor University, Waco, TX 76706, United States

ARTICLE INFO

Keywords:
MoS_2
Scanning tunneling microscope
2D materials
Sputtering
Annealing
Defects

ABSTRACT

Various approaches have been developed to produce MoS_2 monolayers and multilayers. Using plasma and thermal thinning, layer-by-layer thinning processes were developed to produce MoS_2 monolayer and multilayers. However, an atomic-level understanding of the thinning mechanism and defects created in these processes is not clear. In this paper, we studied the impact on surface structures of bulk MoS_2 by argon ion (Ar^+) bombardments and thermal annealing using an ultra-high vacuum (UHV) scanning tunneling microscope (STM). The STM images obtained before and after Ar^+ bombardments show that low-energy (50 eV) Ar^+ ions can remove single atoms from the surface and fragment the top sulfur layer resulting in single sulfur vacancy point defects and atomic pits on the MoS_2 surface. Higher energy (100 eV) Ar^+ ions can penetrate deeper and remove the topmost MoS_2 trilayer. After bombardment with an Ar^+ beam of 500 eV, the MoS_2 surface appeared as granulated nanostructures consisting of 1–3 nm nanoparticles. Upon thermal annealing, topmost sulfur atoms were removed through sublimation after heating at 650 °C for 5 min and deeper atom sublimation was observed with longer annealing time, resulting in granulated nanostructures on the MoS_2 surface.

1. Introduction

The success of graphene has stimulated enthusiasm in the scientific community for other two-dimensional materials with similar properties and structure to graphene. Among the possible materials, molybdenum disulfide (MoS_2) is of particular interest due to its tunable bandgap (between 1.2 and 1.8 eV depending on thickness) [1–3]. MoS_2 is a layered crystal; each layer consists of one hexagonal close-packed Mo atomic layer sandwiched between two atomic layers of hexagonal close-packed S atoms (S − Mo − S) [4]. Atoms within each S − Mo − S trilayer are strongly bonded by covalent interactions. However, the composited tri-layers are held together by weak van der Waals forces, enabling easy layer exfoliation. Few-layer and monolayer MoS_2 show great potential in a wide range of applications for photovoltaics, energy storage, optoelectronics, and catalysis [1–3].

Defects in MoS_2 play an important role in its properties [5–12]. MoS_2 has been shown to exhibit n-type or p-type conduction at different points on the same sample [5]. Qiu et al. [6] reported that in low-carrier-density multilayer MoS_2, the mechanisms of charge transport through defect-induced localized states vary with temperature. Tongay et al. have shown experimental evidence that the presence of zigzag edges, magnetic impurities, and magnetism from sulfur vacancies contribute to ferromagnetic properties in MoS_2 [7]. The edge defects and the sulfur vacancies are also the most reactive sites for the hydrogen evolution reaction [13–17]. In addition to the intrinsic defects, various approaches have been employed to introduce defects to modify the properties of MoS_2 surface [8,9,15,18,19]. The magnetic properties of MoS_2 can be tailored through hydrogenation and proton irradiation [10]. Anion vacancies introduced as a result of α-particles radiation can cause an emergent and enhanced photoluminescence intensity [11,12,20].

Various approaches have been developed to produce single layer or multilayered MoS_2 flakes including scotch tape-based mechanical exfoliation [21], liquid-based exfoliation [22–24] and chemical vapor deposition (CVD) growth [25,26]. New methods such as laser thinning [27], anodic binding [28], focused ion beam [29], thermal thinning [30,31], and plasma thinning [19,32] have been developed in order to obtain MoS_2 monolayer or multilayers in a controlled manner. Both thermal and plasma thinning achieved layer-by-layered reduction of MoS_2 from multilayer to monolayer [30,32]. These methods are also involved in various post processing in applications requiring defect engineering [19,33,34], modification of the electronic structure, and optical properties of MoS_2 monolayer [27,30–32]. However, the impact of plasma thinning and thermal annealing on the atomic structure is not yet clear. To gain a complete understanding of defect formation and layer by layer removal of MoS_2, atomic level studies of these processes

* Corresponding author.
E-mail address: Zhenrong_Zhang@baylor.edu (Z. Zhang).

https://doi.org/10.1016/j.apsusc.2020.147461
Received 27 March 2020; Received in revised form 31 July 2020; Accepted 3 August 2020
Available online 06 August 2020
0169-4332/

are required.

In early studies, Auger electron spectroscopy (AES) [35] and X-ray photoelectron spectroscopy (XPS) [36,37] suggested that basal sulfur atoms were preferentially removed during Ar^+ ion sputtering, resulting in an increase in reactivity. Atomic structure and intrinsic defects on MoS_2 surfaces have been directly observed [38–42] and various Ar^+ ion induced surface defects have been reported using STM [8,9,43]. Removal of sulfur atoms is not observed with argon ions Ar^+ with energies of 100 eV or less although the electronic structure of the MoS_2 surface is altered [43]. Defects produced by Ar^+ ions at higher energies (above 500 eV) appear as dark depressions with various sizes with or without white protrusions on the STM images [8,43]. It was proposed that the removal of the topmost sulfur atoms produced dark depressions and MoS_2 partial layer removal resulted in white protrusions in the STM images [8]. However, direct observation of the removal of single sulfur atoms and MoS_2 layer fragment at an atomic level was not achieved.

In this paper, we studied surface evolution during Ar^+ bombardment and thermal annealing at an atomic level using an ultra-high vacuum (UHV) STM. Our study reveals that the Ar^+ beam of 50 eV can remove topmost sulfur layer resulting in single S vacancies which appear as hexagonal protrusions and remove fractions of the top sulfur layer which appear as surface depressions on STM images. With Ar^+ beam of 100 eV, Ar^+ ions penetrate deeper into MoS_2 lattice and remove up to the top 3 MoS_2 layers. After a 5-s bombardment with Ar^+ beam of 500 eV, a flat MoS_2 surface is replaced by granulated nanostructures consisting of 1–3 nm nanoparticles. Thermal annealing of MoS_2 at 650 °C for 5 min can remove top S atoms from MoS_2 through sublimation. Atoms from deeper layers can be sublimated with longer annealing time, which results in granulated surface nanostructures.

2. Experimental methods

All the bulk MoS_2 used in this study were in the form of the natural mineral molybdenite, acquired from Ward's Natural Science Establishment [44]. MoS_2 samples were peeled with scotch tape to expose fresh MoS_2 surfaces. Freshly peeled MoS_2 samples were mounted onto STM sample holders and transferred into the load lock of the UHV chamber and immediately evacuated. The UHV system (base pressure $< 3 \times 10^{-11}$ Torr) is equipped with a variable temperature STM (SPECS), quadrupole mass spectrometry (SRS), and an ion gun (SPECS). No additional cleaning step was needed for freshly peeled surface. Ideally, the cleaved surface is atomically flat with dangling bonds and defects and is relatively easy to obtain atomic resolution images.

For Ar^+ irradiated samples, the MoS_2 surface was bombarded with Ar^+ ions with energies ranging from 50 eV to 500 eV in an argon partial pressure ranging from 7×10^{-8} torr to 2×10^{-6} torr. Ion currents of about 0.2 μA to 2.5 μA were measured at the sample. For thermal annealing processes, the MoS_2 sample was heated to 650 °C with electron beam heating. STM images were scanned by electrochemically etched W tips and recorded in constant current mode. STM images were acquired with SPECS STM USB software. All STM images (empty states) were collected using constant current (I_t, 0.1–0.3 nA) tunneling mode with a positive sample bias voltage (V_{bias}, 0.4–1.0 V). Atomically resolved images of the initial clean surface state were acquired before Ar^+ bombardment and thermal experiment for each sample. All measurements were carried out at room temperature. The STM images were processed and edited using WSxM software (Nanotech, freeware) [45].

3. Results and discussion

MoS_2 crystals is comprised of a stack of S-Mo-S structures. The top atomic layer of the basal surface is a sheet of sulfur atoms. Fig. 1a depicts a representative large area STM image of the surface of a fresh-cleaved mineral MoS_2 crystal. The most predominate features in Fig. 1a are black concaves with differing contrast that are randomly distributed on the atomically flat basal surface. The STM images clearly shows that most of the dark concaves have a circular shape. The depths of these concaves vary from 0.3 nm to 0.6 nm. An example of the line profile of the defect highlighted with a green square shows a canvas with a depth of 0.5 nm. The root-mean-square (rms) roughness (Z_{rms}) of the Fig. 1a is about 0.5 Å. MoS_2 monolayer steps were also observed as shown in Figure S1a, the thickness of a MoS_2 monolayer measured from STM line profile (Figure S1b) is 0.57 nm, which is very close to the real MoS_2 monolayer thickness of 0.65 nm.

It is needed to point out that the lattice of top surface sulfur atoms and that of molybdenum atoms in the second layer have same structure. Previous STM experiments and theoretical calculations show that only the sulfur atoms on the topmost layer are imaged at low-bias voltages [46–48]. Fig. 1c presents a typical atomically resolved hexagonal pattern of the top sulfur layer (V_{bias} = 10 mV and I_t = 0.25 nA). The hexagonal pattern has a unit cell of 3.1 Å, which is in agreement with the literature results for the 2H phase of MoS_2 [8,38]. Fig. 1d shows an image collected with a different sample bias voltage (V_{bias} = 2.1 V and I_t = 0.25 nA), in which two sets of feature with different contrast can be easily distinguishable. According to a calculation by Gonzalez et al. [49], both S atoms and Mo atoms could be imaged with STM with S atoms shown as brighter contrast and Mo atoms shown as the dimmer contrast when the scanning biases various between 1.9 V and 3.4 V. This is also observed by Addou et al. in their experiments [42]. So we assign the brighter ones as sulfur atoms and the dimmer ones as Mo atoms. In the atomically resolved image (Fig. 1b), the measured depth of the concaves from the inset line profile is 1.8 Å. For most of the features the concave structures are superimposed with a perfect sulfur lattice, indicating that dark concave defects are likely caused by local subsurface dopants other than morphological effects [50]. An earlier study showed that there were no surface defects observed with atomic force microscopy (AFM); however, concave features were observed on the same area of the MoS_2 surface using STM [40]. As presented, in large area STM images (Fig. 1a) and supporting images (Figure S1a, Figure S1b, and Figure S2), the area density of the black concaves varies not only with different samples but also with different locations on the same surface. In Figure S1b, the density of the black concaves from the up-right corner and the low-left corner are ~ 9% and ~ 0.5%, respectively. This is consistent with Addou et al.'s results that the area density can vary from 10% to 1.5% [42].

The top layer surface sulfur atoms can be removed with low energy (50 eV) Ar^+ ion bombardment. Fig. 2a shows a large area STM images of MoS_2 surface after a 5 s bombardments with 50 eV Ar^+ beam. The root-mean-square (rms) roughness (Z_{rms}) increased from ~ 0.49 Å on fresh samples to ~ 0.74 Å. The smaller, higher resolution image shows that two types of distinct features appeared after 5 s of Ar^+ sputtering (Fig. 2b). The first type of feature are bright protrusions (highlighted with blue rectangle). The atomically resolved image shows that the bright protrusions have a bright hexagonal ring surrounded by dark area. The size of the rings is uniform and their diameter is ~ 2 nm including the surrounding dark area (Fig. 2c). Six S atoms can be individually identified. The diagonal distance (0.7 nm) between the apexes of the hexagonal ring is about twice that of the lattice constant of MoS_2. The line profile (green line in Fig. 2d) shows that the height difference between the ring and the center of the ring is ~ 2 Å, indicating the removal of a single S atom to form a point defect in the center of the hexagonal ring (see Figure S5 for more images and line profiles of sulfur vacancy point defects). The depth of sulfur vacancy defect agrees with what is expected and what has been reported (~1.9 Å) for the sulfur vacancy defect in reference [42]. The second type of feature are black pits (highlighted in green circle in Fig. 2b) with various shapes. The new black pits (Fig. 2e) are shallow and their periphery are not circular or consistent as the intrinsic black concaves widely observed in natural molybdenite (Fig. 1a). In the images with atomic resolution (Fig. 2e), it can be seen that the ordered structure still remains inside the pits. It is necessary to point out that characteristic

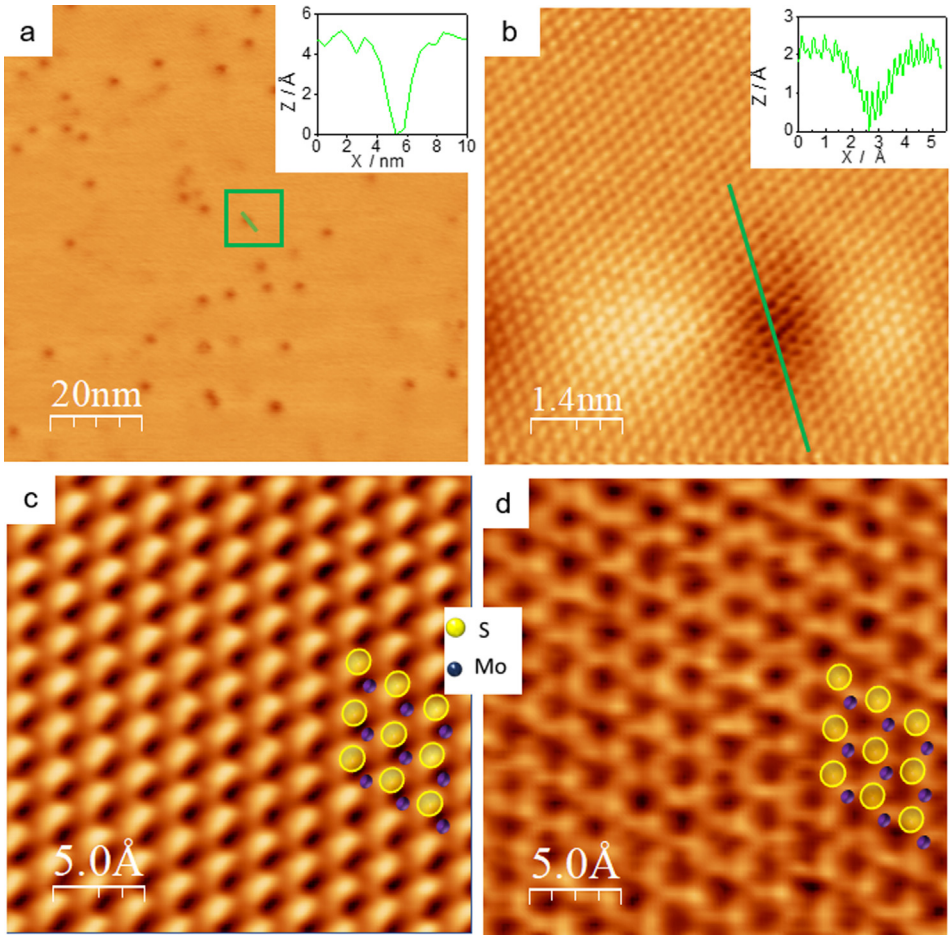

Fig. 1. STM images of the freshly peeled MoS_2 (0001) surface. a: Large area (100 nm × 100 nm) STM image exhibits dark defects (V_{bias} = 590 mV, I_t = 0.14 nA). The inserted line profile was taken across the dark defect inside the green rectangle. b: Atomic resolution image of area outlined in image Fig. 1a by the green rectangle box. (V_{bias} = 590 mV, I_t = 0.14 nA). The inset line profile was from the green line. c: Atomically resolved STM image showing top layer S atoms with hexagonal pattern (V_{bias} = 10 mV, I_t = 0.25 nA). d: High resolution STM image showing both S- and Mo-layer structure presented different contrast, respectively. (V_{bias} = 2.1 V, I_t = 0.25 nA). The positions of sulfur atoms (yellow circles) and molybdenum atoms (blue circles) are highlighted in both images. Additional atomic resolution images at relatvily low biases are presented in Figure S2. (For interpretation of the references to colour in this figure legend, the reader is referred to the web version of this article.)

distortions at the bottom of some of the STM images (Fig. 2c and in Fig. 2e) are due to tip drift which is nearly inevitable in the STM imaging process when the direction of the tip motion is reversed. Similarly, external vibration introduces occasional noise in the STM images which appears as streaks in Fig. 2e. This is especially common in the images with atomic resolution. Line profiles (Fig. 2f) show that the depth of the newly formed pits is around 2 Å as well (see Figures S5 and S6 for more images and line profiles collected with different parameters). The irregular shape of the black pits and the depths of the pits strongly suggest that portions of the top layer of the sulfur atom sheet were removed under Ar^+ bombardment. When the acceleration voltage is increased, the Ar^+ ions with higher energy cause more damage to the MoS_2 surface. Fig. 3a presents large area STM images of MoS_2 after 5 s of Ar^+ ion bombardment with an energy of 100 eV. The surface is clearly rougher; the root-mean-square (rms) roughness (Z_{rms}) increased to ~ 2.65 Å. The MoS_2 surface now exhibits hill and valley structures. In the images with atomic resolution (Fig. 3b), the hills still show atomic pattern of MoS_2, which indicates that these were less bombarded area, the valleys show more damages by Ar^+ beams.

The line profiles (Fig. 3c) show that the depth is ~ 0.7 nm in some areas (green line), which corresponds to removal of one MoS_2 tri-layer and in other areas (blue line) the depth of the valley is ~ 2.1 nm corresponding to three MoS_2 tri-layers. Figure S7 shows additional STM images and line profiles.

After bombardment with higher energy (500 eV) Ar^+ ions for 5 s (Fig. 3d-f), the ordered surface structure of MoS_2 surface is completely transformed into a granulated structure. The surface is covered with nanoparticles with sizes about 1 ~ 3 nm (Fig. 3e and Fig. 3f). The line profile confirms that the depth of the granulated structure is about 3 nm (Figures S7c and S7d).

Previous reports of STM investigations on Ar^+ ion bombarded MoS_2 show that defects can be produced with energies of 500 eV [8] and 1 keV [9] and the granulated nanostructure has not yet been reported on MoS_2. After 1 min of Ar^+ bombardments at 500 eV, the MoS_2 surface is fully transformed into granulated structures with larger nanoparticles (10 ~ 15 nm) (Fig. 3g). Again, there is distortion in Fig. 3g caused by drift during the imaging process. High resolution images confirm that these larger nanoparticles consist of smaller nanoparticles with diameters of 1–3 nm (Fig. 3h and i). The MoS_2 surface became rougher and the depth of the surface nanostructures is about 7 nm (Figures S7e and S7f).

Although it is well known that energetic particles can induce surface damage and surface deformation, it is a surprise that Ar^+ ions with energies as low as 50 eV not only induce single sulfur vacancies on the MoS_2 surfaces but they can also knock off fractions of the top layer of S atoms. This indicates that the 2D nature of MoS_2 plays an important role in the defect formation process. Ar^+ ions with 100 eV can penetrate deeper and remove three MoS_2 tri-layers. This indicates that it is crucial to optimize the energy of Ar^+ beams for controlled layer-by-layer thinning process and for preparing surfaces with desired defects or structure. High energy Ar^+ ions induce nanoparticles on MoS_2, which is not favorable in the MoS_2 plasma thinning process as the removal of the top layers is uneven and may limit the production of monolayer or multilayers. The resultant defects and inhomogeneous surface from sputtering could be useful in studying defects related catalytic, optical, electronic, and magnetic properties [51,52].

The thermal stability of MoS_2 is important as it is related to the fabrication and application of MoS_2 monolayer and multilayers. Many electronic components for control systems and sensors are required to operate at high temperature [53]. MoS_2 monolayer can be achieved by

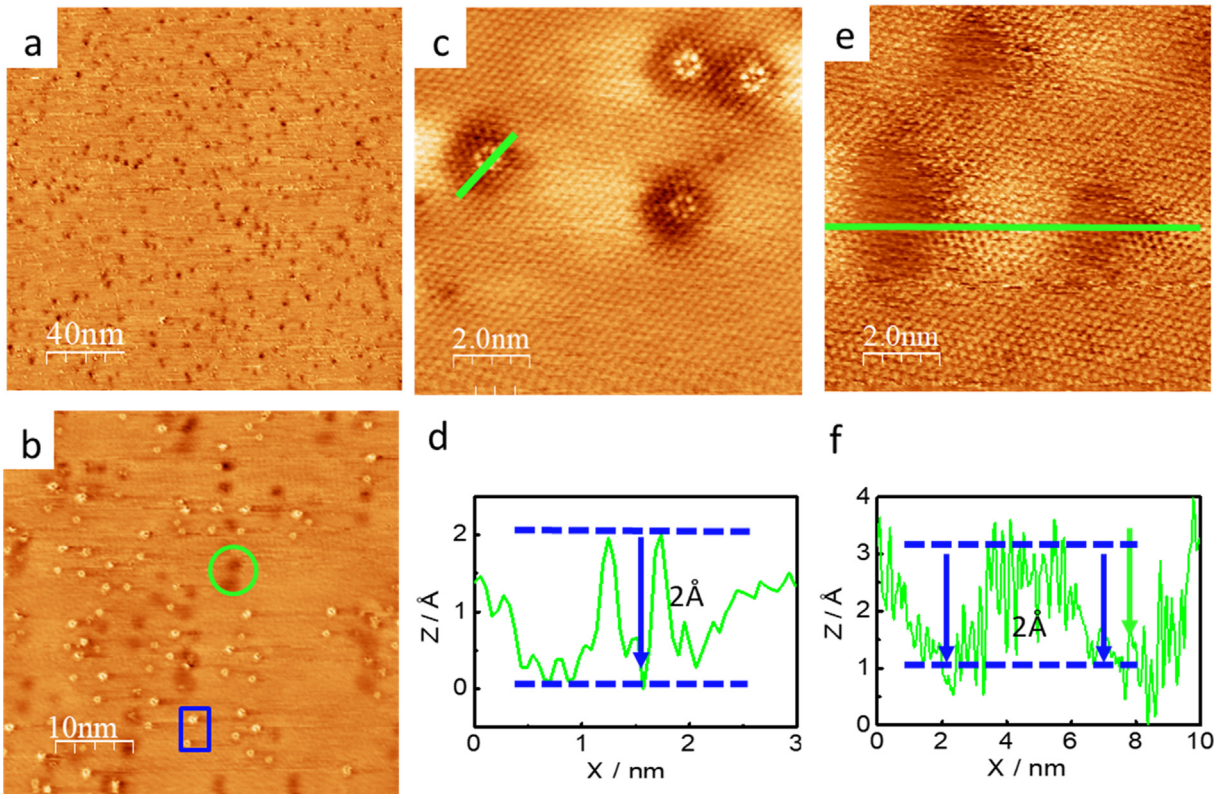

Fig. 2. STM images of MoS_2 after Ar^+ sputtering. a: Large area STM image (V_{bias} = 1350 mV, I_t = 0.25 nA) after 50 eV Ar^+ bombardment. Sputtering parameters: $P = 7.2 \times 10^{-8}$ torr, E = 50 eV, *time* = 5 s. b: Enlarged STM image of MoS_2 after 50 eV Ar^+ bombardment showing addition of white rings and black concaves. c and d: Atomic resolution STM image (V_{bias} = 670 mV, I_t = *0.*45 nA) and line profile showing the detailed hexagonal ring structures caused by 50 eV Ar^+ bombardment. e and f: Atomic resolution STM image and line profile showing areas with top layer S atoms removed by 50 eV Ar^+ beam. Additional line profiles of single sulfur vacancies are presented in Figure S5 and Figure S6.

layer by layer thinning when annealed in argon atmosphere at 650 °C.[21] Optical properties (e.g. photoluminescence) of MoS_2 monolayer could be dramatically enhanced by cracks/defects formed during high-temperature annealing (500 °C) in vacuum [34]. To exam the structural changing in thermal annealing, bulk MoS_2 was annealed at 650 °C in vacuum and scanned with STM after cooling to room temperature. Fig. 4a represents the clean surface of the freshly peeled MoS_2 surface with a low density of intrinsic defects before annealing. After annealing at 650 °C for 5 min, a high density of black pits (21% of surface area) appeared in large area STM image (Fig. 4b). The size and shape of the black pit are not as uniform as the intrinsic defects. In the images with atomic resolution, we can see that the ordered atomic structure remained after annealing. The line profile shows that the depth of most of the newly appeared pits is ~ 2 Å (Fig. 4h), which indicates that top layer sulfur atoms were removed by thermal sublimation. Fig. 4c shows that the MoS_2 surface became corrugated after a 10 min annealing at 650 °C. The surface appears comparable to the surface sputtered by 100 eV Ar^+ beam (Fig. 3a). With atomic resolution imaging, it can be clearly seen that several defect spots reach each other and form a bigger feature which appear as valley in lower resolution image (highlighted in blue rectangle in Fig. 4f and 3D STM image in Figure S4b). The line profile shows that depths of the deeper pit is around 6.4 Å, which corresponds to the thickness of a single MoS_2 tri-layer. Additional images and line profiles collected with different parameters are presented in Figure S9. Another line profile (with depth of ~ 1.8 Å Figure S4c) shows areas in which the top layer sulfur atoms were removed by thermal sublimation. The RMS roughness of fresh sample surface was 0.15 Å and increased to Z_{rms} = 0.5 Å after 10 min thermal annealing and Z_{rms} = 1.5 Å after 20 min thermal annealing (Figure S3). Our STM observation shows that the sublimation of bulk MoS_2 surface is not even at the atomic level. Surface sulfur atoms and top layer MoS_2 can be removed simultaneously during the same thermal annealing process. Large scale (micrometer) uneven sublimation of surfaces was reported during thermal thinning of MoS_2 nanoflakes in argon [30]. Double layer MoS_2 were removed in some areas while monolayer was removed in other areas within one thermal cycle, which results in inhomogeneous nanoflakes. In the annealing of double layer MoS_2 in air [31], the uneven etching of MoS_2 produced meshed MoS_2 sheet with MoO_3 impurities. Although areas with flat a surface can be achieved on MoS_2 [31], our results indicate that the uneven sublimation nature at the atomic level in MoS_2 thermal thinning process should be considered. Similar to the effect of argon sputtering, the rough surface caused by uneven thermal sublimation on MoS_2 may limit its viability in producing MoS_2 monolayer or multilayers. Since thermal thinning and Ar^+ plasma thinning are different physical processes and involve different mechanisms, it is unexpected that both processes would introduce similar surface defects and nanostructures on the MoS_2 surfaces. However, the uneven sublimation and argon sputtering result in surface defects with abundant dangling bonds and increased surface areas which provide feasible methods to generate MoS_2 with the desired surface defects for HER catalysis [13,14]. The uneven sublimation will also altered the charge transport in the layered structure and the magnetism from sulfur vacancies which in turn affect its optoelectronic and spintronic applications [6,54].

4. Conclusion

We have studied the contribution of Ar^+ ion bombardment and thermal annealing on the surface modification of MoS_2 surfaces with scanning tunneling microscopy. Our results show that during the thermal thinning or Ar^+ plasma thinning process, the MoS_2 surface roughness increases as top layer sulfur atoms or MoS_2 tri-layers are

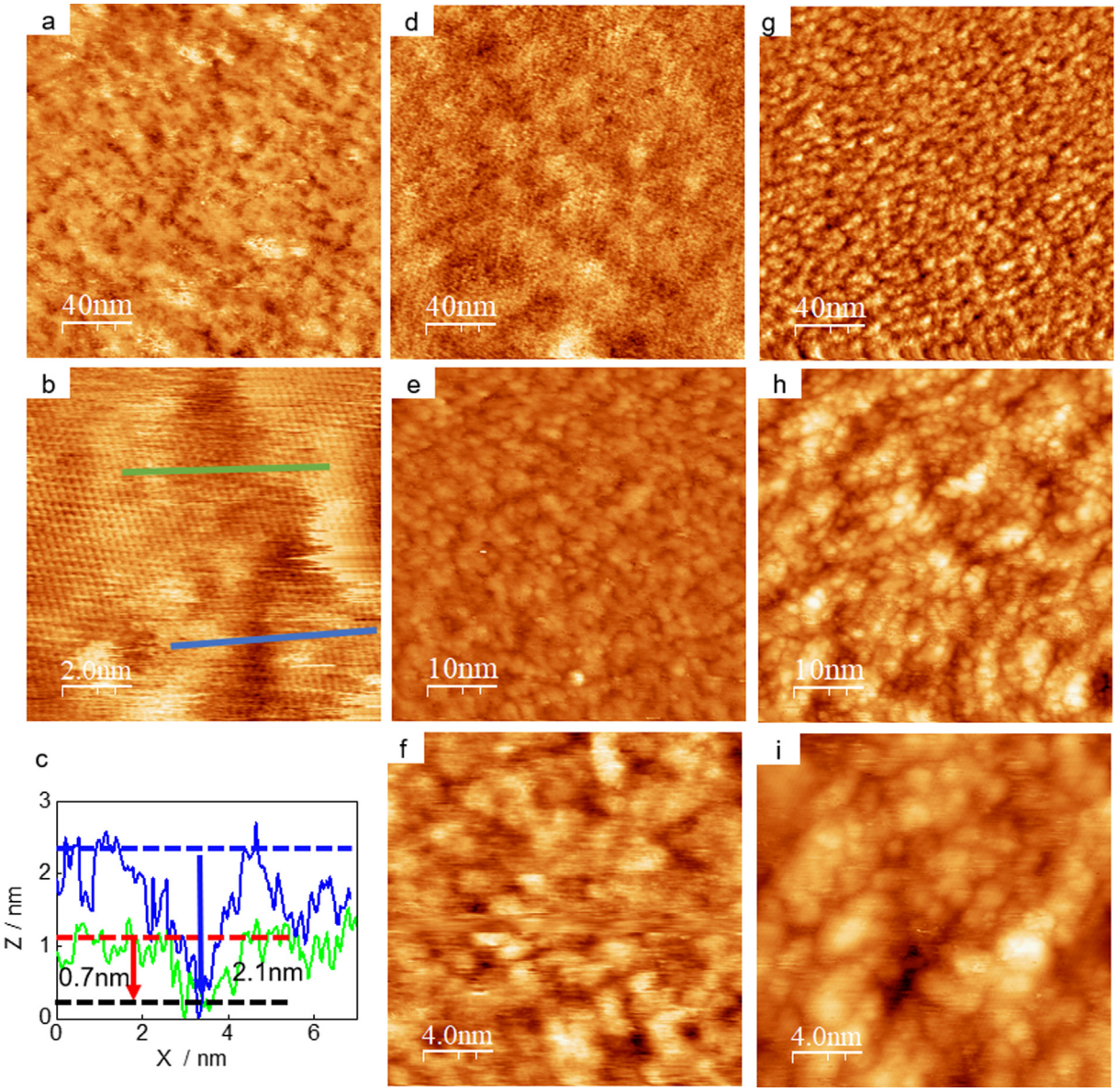

Fig. 3. STM images of MoS_2 after Ar^+ sputtering with 100 eV and 500 eV. a: Large area STM image of MoS_2 sputtered at 100 eV (Sputtering parameters: $P = 7.2 \times 10^{-8}$ torr, $E = 100$ eV, $I = 10$ mA, $I_{read} = 0.2$ μA, *time* = 6 s) b: Atomic resolution image of a. c: Line profiles from areas with one MoS_2 layer (green line) removed and two MoS_2 layers removed (blue line) d-f: STM images of MoS_2 sputtered for 5 s at 500 eV (Sputtering parameters: $P = 1.0 \times 10^{-7}$ torr, $E = 500$ eV, *time* = 5 s); g-i: STM images of MoS_2 sputtered for 1 min at 500 eV (sputtering parameters: $P = 1.8 \times 10^{-6}$ torr, $E = 500$ eV, *time* = 1 min).

removed by sputtering or sublimation. With 50 eV Ar^+ beam, single top layer sulfur atoms or fractions of the top layer of sulfur atoms can be removed resulting in single sulfur vacancy point defects appearing as hexagonal patterns or black pits in STM images. The topmost MoS_2 tri-layer as well as second tri-layer can be removed by Ar^+ ions with higher energy (100 eV). Granulated nanostructures were produced with 500 eV Ar^+ bombardments. Similarly, top layer sulfur atoms can be sublimated through annealing at 650 °C in vacuum and granulated nanostructures were observed on MoS_2 surface with 20 min annealing at the same temperature. The defects introduced and the resultant nanostructured inhomogeneous surface may provide pathways for engineering substrates for catalytic applications of MoS_2. Our findings provide new insights at the atomic level on the point defects and the granulated nanostructures introduced due to thermal annealing and interactions between energetic particles and MoS_2 surfaces. Such structural changes can affect the chemical, electric, magnetic, and optical properties of MoS_2 and impact its applications in various fields including photovoltaics, energy storage, optoelectronics, and catalysis.

Declaration of Competing Interest

The authors declare that they have no known competing financial interests or personal relationships that could have appeared to influence the work reported in this paper.

Acknowledgement

Acknowledgment is made to the Donors of the American Chemical Society Petroleum Research Fund, United States for partial support of this research. This work was partially supported by the National Science Foundation, United States under Grant CHE-1609608, CHE-1905043 and the Office of vice Provost for Research of Baylor University, United States.

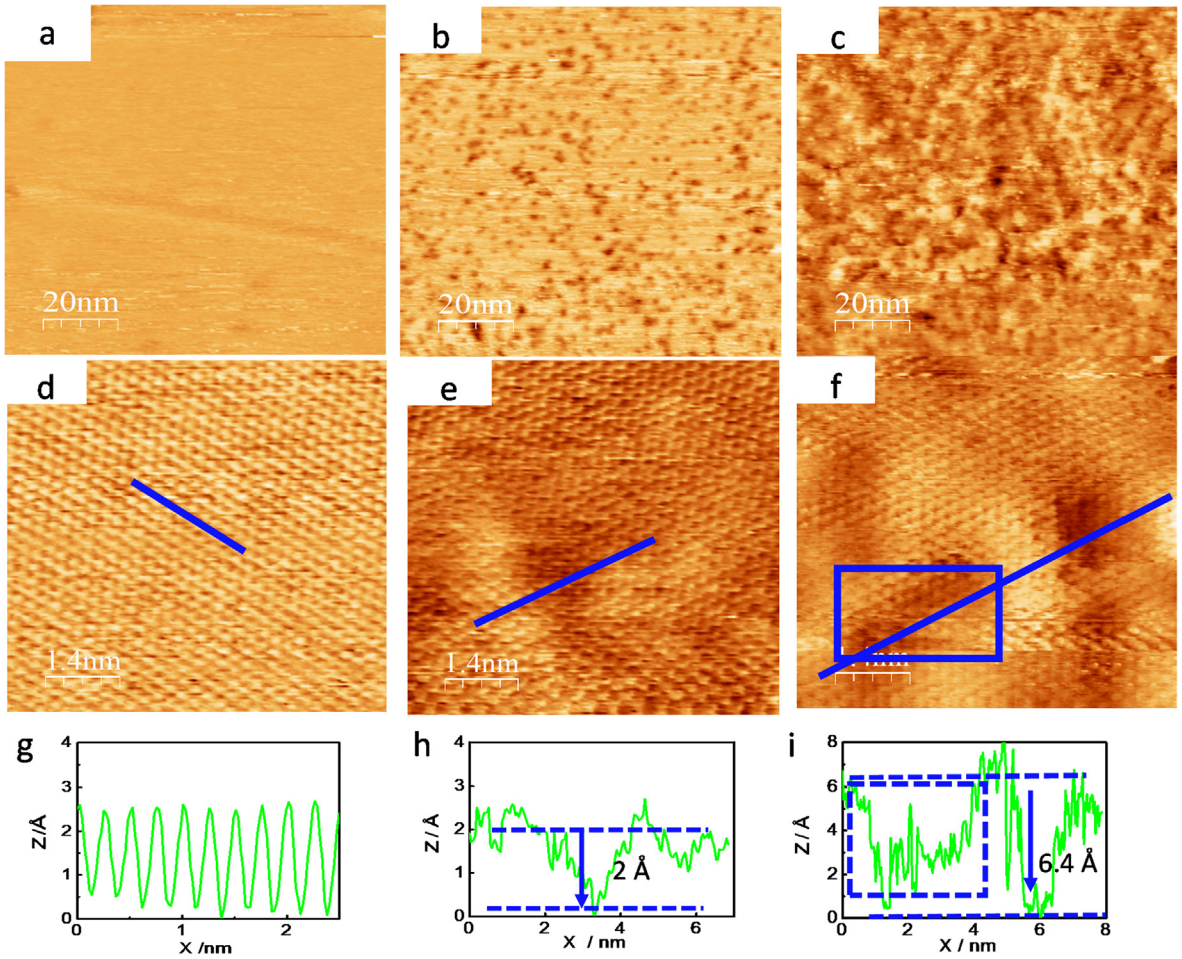

Fig. 4. Annealing effect on MoS_2 surface. a: Large area STM images of original surface (V_{bias} = 1250 mV, I_t = 0.12 nA); b: Large area STM images of MoS_2 surface (V_{bias} = 1480 mV, I_t = 0.17 nA) annealed at 650 °C for 5 min; c: Large area STM image of MoS_2 surface (V_{bias} = 640 mV, I_t = 0.18 nA) annealed at 650 °C for 10 min; d: Atomic resolution STM image of original surface (V_{bias} = 880 mV, I_t = 0.15 nA); e: Atomic resolution image of b (V_{bias} = 740 mV, I_t = 0.12 nA); f: Atomic resolution images of c; g: Line profile of d; h: Line profile of e showing that the depth (~2.0 Å) of the defects; i: Line profile of f showing that the depth (~6.4 Å) of blue line. Additional line profiles are presented in Figure S9. (For interpretation of the references to colour in this figure legend, the reader is referred to the web version of this article.)

Appendix A. Supplementary material

Supplementary data to this article can be found online at https://doi.org/10.1016/j.apsusc.2020.147461.

References

[1] M. Bernardi, M. Palummo, J.C. Grossman, Extraordinary Sunlight Absorption and One Nanometer Thick Photovoltaics Using Two-Dimensional Monolayer Materials, Nano Lett. 13 (2013) 3664–3670, https://doi.org/10.1021/nl401544y.
[2] K. Chang, W. Chen, L-Cysteine-Assisted Synthesis of Layered MoS_2/Graphene Composites with Excellent Electrochemical Performances for Lithium Ion Batteries, ACS Nano. 5 (2011) 4720–4728, https://doi.org/10.1021/nn200659w.
[3] D. Jariwala, V.K. Sangwan, L.J. Lauhon, T.J. Marks, M.C. Hersam, Emerging Device Applications for Semiconducting Two-Dimensional Transition Metal Dichalcogenides, ACS Nano. 8 (2014) 1102–1120, https://doi.org/10.1021/nn500064s.
[4] R. Dickinson, L. Pauling, The crystal structure of molybdenite, J. Am. Chem. Soc. 45 (1923) 1466–1471, https://doi.org/10.1021/ja01659a020.
[5] S. McDonnell, R. Addou, C. Buie, R.M. Wallace, C.L. Hinkle, Defect-Dominated Doping and Contact Resistance in MoS_2, ACS Nano. 8 (2014) 2880–2888, https://doi.org/10.1021/nn500044q.
[6] H. Qiu, T. Xu, Z. Wang, W. Ren, H. Nan, Z. Ni, Q. Chen, S. Yuan, F. Miao, F. Song, G. Long, Y. Shi, L. Sun, J. Wang, X. Wang, Hopping transport through defect-induced localized states in molybdenum disulphide, Nat. Commun. 4 (2013) 2642, https://doi.org/10.1038/ncomms3642.
[7] S. Tongay, S.S. Varnoosfaderani, B.R. Appleton, J. Wu, A.F. Hebard, Magnetic properties of MoS_2: Existence of ferromagnetism, Appl. Phys. Lett. 101 (2012) 123105, , https://doi.org/10.1063/1.4753797.
[8] A. Inoue, T. Komori, K. Shudo, Atomic-scale structures and electronic states of defects on Ar^+-ion irradiated MoS_2, J. Electron Spectrosc. Relat. Phenom. 189 (2013) 11–18, https://doi.org/10.1016/j.elspec.2012.12.005.
[9] N. Sengoku, K. Ogawa, Investigations of Electronic-Structures of Defects Introduced by Ar Ion Bombardments on MoS_2 by Scanning Tunneling Microscopy, Jpn. J. Appl. Phys. Part 1 - Regul. Pap. Short Notes Rev. Pap. 34 (1995) 3363–3367, https://doi.org/10.1143/JJAP.34.3363.
[10] S.W. Han, Y.H. Hwang, S. Kim, W.S. Yun, J.D. Lee, M.G. Park, S. Ryu, J.S. Park, D. Yoo, S. Yoon, S.C. Hong, K.S. Kim, Y.S. Park, Controlling Ferromagnetic Easy Axis in a Layered MoS_2 Single Crystal, Phys. Rev. Lett. 110 (2013) 247201, , https://doi.org/10.1103/PhysRevLett.110.247201.
[11] T. Korn, S. Heydrich, M. Hirmer, J. Schmutzler, C. Schueller, Low-temperature photocarrier dynamics in monolayer MoS_2, Appl. Phys. Lett. 99 (2011) 102109, , https://doi.org/10.1063/1.3636402.
[12] S. Tongay, J. Suh, C. Ataca, W. Fan, A. Luce, J.S. Kang, J. Liu, C. Ko, R. Raghunathanan, J. Zhou, F. Ogletree, J. Li, J.C. Grossman, J. Wu, Defects activated photoluminescence in two-dimensional semiconductors: interplay between bound, charged, and free excitons, Sci Rep. 3 (2013) 2657, https://doi.org/10.1038/srep02657.
[13] Y. Yin, J. Han, Y. Zhang, X. Zhang, P. Xu, Q. Yuan, L. Samad, X. Wang, Y. Wang, Z. Zhang, P. Zhang, X. Cao, B. Song, S. Jin, Contributions of Phase, Sulfur Vacancies, and Edges to the Hydrogen Evolution Reaction Catalytic Activity of Porous Molybdenum Disulfide Nanosheets, J. Am. Chem. Soc. 138 (2016) 7965–7972, https://doi.org/10.1021/jacs.6b03714.
[14] J. Zhu, Z. Wang, H. Dai, Q. Wang, R. Yang, H. Yu, M. Liao, J. Zhang, W. Chen, Z. Wei, N. Li, L. Du, D. Shi, W. Wang, L. Zhang, Y. Jiang, G. Zhang, Boundary activated hydrogen evolution reaction on monolayer MoS_2, Nat. Commun. 10 (2019) 1348, https://doi.org/10.1038/s41467-019-09269-9.
[15] C. Sun, P. Wang, H. Wang, C. Xu, J. Zhu, Y. Liang, Y. Su, Y. Jiang, W. Wu, E. Fu, G. Zou, Defect engineering of molybdenum disulfide through ion irradiation to boost hydrogen evolution reaction performance, Nano Res. 12 (2019) 1613–1618,

https://doi.org/10.1007/s12274-019-2400-1.
[16] R. Wang, Q. Shao, Q. Yuan, P. Sun, R. Nie, X. Wang, Direct growth of high-content 1T phase MoS_2 film by pulsed laser deposition for hydrogen evolution reaction, Appl. Surf. Sci. 504 (2020) 144320, , https://doi.org/10.1016/j.apsusc.2019.144320.
[17] Y. Liu, Z. Gong, Y. Xie, H. Lv, B. Zhang, Revealing the synergetic effects of graphene and MoS_2 on boosted photocatalytic H_2 production of $Mn_{0.5}Cd_{0.5}S$ photocatalyst, Appl. Surf. Sci. 505 (2020) 144637, , https://doi.org/10.1016/j.apsusc.2019.144637.
[18] Y. Chen, S. Huang, X. Ji, K. Adepalli, K. Yin, X. Ling, X. Wang, J. Xue, M. Dresselhaus, J. Kong, B. Yildiz, Tuning Electronic Structure of Single Layer MoS_2 through Defect and Interface Engineering, ACS Nano. 12 (2018) 2569–2579, https://doi.org/10.1021/acsnano.7b08418.
[19] B. Huang, F. Tian, Y. Shen, M. Zheng, Y. Zhao, J. Wu, Y. Liu, S.J. Pennycook, J.T.L. Thong, Selective Engineering of Chalcogen Defects in MoS_2 by Low-Energy Helium Plasma, ACS Appl. Mater. Interfaces. 11 (2019) 24404–24411, https://doi.org/10.1021/acsami.9b05507.
[20] J. Li, S. Hu, Z. Chen, Y. Liang, H. Kang, Y. Zhang, Y. Sui, S. Wang, G. Yu, S. Peng, Z. Jin, X. Liu, Facile and rigorous route to distinguish the boundary structure of monolayer MoS_2 domains by oxygen etching, Appl. Surf. Sci. 510 (2020) 145412, , https://doi.org/10.1016/j.apsusc.2020.145412.
[21] K. Novoselov, D. Jiang, F. Schedin, T. Booth, V. Khotkevich, S. Morozov, A. Geim, Two-dimensional atomic crystals, Proc. Natl. Acad. Sci. U. S. A. 102 (2005) 10451–10453, https://doi.org/10.1073/pnas.0502848102.
[22] J.N. Coleman, M. Lotya, A. O'Neill, S.D. Bergin, P.J. King, U. Khan, K. Young, A. Gaucher, S. De, R.J. Smith, I.V. Shvets, S.K. Arora, G. Stanton, H. Kim, K. Lee, G.T. Kim, G.S. Duesberg, T. Hallam, J.J. Boland, J.J. Wang, J.F. Donegan, J.C. Grunlan, G. Moriarty, A. Shmeliov, R.J. Nicholls, J.M. Perkins, E.M. Grieveson, K. Theuwissen, D.W. McComb, P.D. Nellist, V. Nicolosi, Two-Dimensional Nanosheets Produced by Liquid Exfoliation of Layered Materials, Science. 331 (2011) 568–571, https://doi.org/10.1126/science.1194975.
[23] R.J. Smith, P.J. King, M. Lotya, C. Wirtz, U. Khan, S. De, A. O'Neill, G.S. Duesberg, J.C. Grunlan, G. Moriarty, J. Chen, J. Wang, A.I. Minett, V. Nicolosi, J.N. Coleman, Large-Scale Exfoliation of Inorganic Layered Compounds in Aqueous Surfactant Solutions, Adv Mater. 23 (2011) 3944-+, https://doi.org/10.1002/adma.201102584.
[24] R. Zhang, X. Yang, J. Pu, Z. He, L. Xiong, Extraordinary macroscale lubricity of sonication-assisted fabrication of MoS_2 nano-ball and investigation of in situ formation mechanism of graphene induced by tribochemical reactions, Appl. Surf. Sci. 510 (2020) 145456, , https://doi.org/10.1016/j.apsusc.2020.145456.
[25] K. Liu, W. Zhang, Y. Lee, Y. Lin, M. Chang, C. Su, C. Chang, H. Li, Y. Shi, H. Zhang, C. Lai, L. Li, Growth of Large-Area and Highly Crystalline MoS_2 Thin Layers on Insulating Substrates, Nano Lett. 12 (2012) 1538–1544, https://doi.org/10.1021/nl2043612.
[26] Y. Lin, W. Zhang, J. Huang, K. Liu, Y. Lee, C. Liang, C. Chu, L. Li, Wafer-scale MoS_2 thin layers prepared by MoO_3 sulfurization, Nanoscale. 4 (2012) 6637–6641, https://doi.org/10.1039/c2nr31833d.
[27] A. Castellanos-Gomez, M. Barkelid, A.M. Goossens, V.E. Calado, H.S.J. van der Zant, G.A. Steele, Laser-Thinning of MoS_2: On Demand Generation of a Single-Layer Semiconductor, Nano Lett. 12 (2012) 3187–3192, https://doi.org/10.1021/nl301164v.
[28] K. Gacem, M. Boukhicha, Z. Chen, A. Shukla, High quality 2D crystals made by anodic bonding: a general technique for layered materials, Nanotechnology. 23 (2012) 505709, , https://doi.org/10.1088/0957-4484/23/50/505709.
[29] D. Wang, Y. Wang, X. Chen, Y. Zhu, K. Zhan, H. Cheng, X. Wang, Layer-by-layer thinning of two-dimensional MoS_2 films by using a focused ion beam, Nanoscale. 8 (2016) 4107–4112, https://doi.org/10.1039/c5nr05768j.
[30] X. Lu, M.I.B. Utama, J. Zhang, Y. Zhao, Q. Xiong, Layer-by-layer thinning of MoS_2 by thermal annealing, Nanoscale. 5 (2013) 8904–8908, https://doi.org/10.1039/c3nr03101b.
[31] J. Wu, H. Li, Z. Yin, H. Li, J. Liu, X. Cao, Q. Zhang, H. Zhang, Layer Thinning and Etching of Mechanically Exfoliated MoS_2 Nanosheets by Thermal Annealing in Air, Small. 9 (2013) 3314–3319, https://doi.org/10.1002/smll.201301542.
[32] Y. Liu, H. Nan, X. Wu, W. Pan, W. Wang, J. Bai, W. Zhao, L. Sun, X. Wang, Z. Ni, Layer-by-Layer Thinning of MoS_2 by Plasma, ACS Nano. 7 (2013) 4202–4209, https://doi.org/10.1021/nn400644t.
[33] B. Birmingham, J. Yuan, M. Filez, D. Fu, J. Hu, J. Lou, M.O. Scully, B.M. Weckhuysen, Z. Zhang, Probing the Effect of Chemical Dopant Phase on Photoluminescence of Monolayer MoS_2 Using in Situ Raman Microspectroscopy, J. Phys. Chem. C. 123 (2019) 15738–15743, https://doi.org/10.1021/acs.jpcc.9b03277.
[34] H. Nan, Z. Wang, W. Wang, Z. Liang, Y. Lu, Q. Chen, D. He, P. Tan, F. Miao, X. Wang, J. Wang, Z. Ni, Strong Photoluminescence Enhancement of MoS_2 through Defect Engineering and Oxygen Bonding, ACS Nano. 8 (2014) 5738–5745, https://doi.org/10.1021/nn500532f.
[35] R. Williams, A. Mcevoy, Some Properties of Molybdenite Cleavage Surfaces, J. Phys. D-Appl. Phys. 4 (1971) 456–1000, https://doi.org/10.1088/0022-3727/4/3/316.
[36] J. Lince, D. Csrre, P. Fleischauer, Effects of Argon Ion-Bombardment on the Basal-Plane Surface of MoS_2, Langmuir. 2 (1986) 805–808, https://doi.org/10.1021/la00072a026.
[37] M. Baker, R. Gilmore, C. Lenardi, W. Gissler, XPS investigation of preferential sputtering of S from MoS_2 and determination of MoS_x stoichiometry from Mo and S peak positions, Appl. Surf. Sci. 150 (1999) 255–262, https://doi.org/10.1016/S0169-4332(99)00253-6.
[38] G. Stupian, M. Leung, Imaging of MoS_2 by Scanning Tunneling Microscopy, Appl. Phys. Lett. 51 (1987) 1560–1562, https://doi.org/10.1063/1.98635.
[39] D. Sarid, T. Henson, N. Armstrong, L. Bell, Probing of Basal Planes of Mos_2 by Scanning Tunneling Microscopy, Appl. Phys. Lett. 52 (1988) 2252–2254, https://doi.org/10.1063/1.99769.
[40] W. Heckl, F. Ohnesorge, G. Binnig, M. Specht, M. Hashmi, Ring Structures on Natural Molybdenum-Disulfide Investigated by Scanning Tunneling and Scanning Force Microscopy, J. Vac. Sci. Technol. B. 9 (1991) 1072–1078, https://doi.org/10.1116/1.585263.
[41] H. Permana, S. Lee, K. Ng, Observation of Protrusions and Ring Structures on MoS_2 by Scanning Tunneling Microscopy, J. Vac. Sci. Technol. B. 10 (1992) 2297–2301, https://doi.org/10.1116/1.586057.
[42] R. Addou, L. Colombo, R.M. Wallace, Surface Defects on Natural MoS_2, ACS Appl. Mater. Interfaces. 7 (2015) 11921–11929, https://doi.org/10.1021/acsami.5b01778.
[43] J. Park, C. France, B. Parkinson, Scanning tunneling microscopy investigation of nanostructures produced by Ar^+ and He^+ bombardment of MoS_2 surfaces, J. Vac. Sci. Technol. B. 23 (2005) 1532–1542, https://doi.org/10.1116/1.1993622.
[44] K. Park, M. Richards-Babb, M. Freund, J. Weiss, K. Klier, Surface structure of single-crystal MoS_2(0002) and Cs/MoS_2(0002) by X-ray photoelectron diffraction, J. Phys. Chem. 100 (1996) 10739–10745, https://doi.org/10.1021/jp9605865.
[45] I. Horcas, R. Fernandez, J.M. Gomez-Rodriguez, J. Colchero, J. Gomez-Herrero, A.M. Baro, WSXM: A software for scanning probe microscopy and a tool for nanotechnology, Rev. Sci. Instrum. 78 (2007) 013705, , https://doi.org/10.1063/1.2432410.
[46] A. Altibelli, C. Joachim, P. Sautet, Interpretation of STM images: The MoS_2 surface, Surf. Sci. 367 (1996) 209–220, https://doi.org/10.1016/S0039-6028(96)00864-3.
[47] S. Helveg, J. Lauritsen, E. Laegsgaard, I. Stensgaard, J. Norskov, B. Clausen, H. Topsoe, F. Besenbacher, Atomic-scale structure of single-layer MoS_2 nanoclusters, Phys. Rev. Lett. 84 (2000) 951–954, https://doi.org/10.1103/PhysRevLett.84.951.
[48] K. Kobayashi, J. Yamauchi, Electronic-Structure and Scanning-Tunneling-Microscopy Image of Molybdenum Dichalcogenide Surfaces, Phys. Rev. B. 51 (1995) 17085–17095, https://doi.org/10.1103/PhysRevB.51.17085.
[49] C. Gonzalez, B. Biel, Y.J. Dappe, Theoretical characterisation of point defects on a MoS_2 monolayer by scanning tunnelling microscopy, Nanotechnology. 27 (2016) 105702, , https://doi.org/10.1088/0957-4484/27/10/105702.
[50] T. Matthes, C. Sommerhalter, A. Rettenberger, P. Bruker, J. Boneberg, M. Lux-Steiner, P. Leiderer, Imaging of dopants in surface and sub-surface layers of the transition metal dichalcogenides WS_2 and WSe_2 by scanning tunneling microscopy, Appl. Phys. A-Mater. Sci. Process. 66 (1998) S1007–S1011, https://doi.org/10.1007/s003390051285.
[51] G. Li, D. Zhang, Q. Qiao, Y. Yu, D. Peterson, A. Zafar, R. Kumar, S. Curtarolo, F. Hunte, S. Shannon, Y. Zhu, W. Yang, L. Cao, All The Catalytic Active Sites of MoS_2 for Hydrogen Evolution, J. Am. Chem. Soc. 138 (2016) 16632–16638, https://doi.org/10.1021/jacs.6b05940.
[52] F. Ling, X. Liu, H. Jing, Y. Chen, W. Zeng, Y. Zhang, W. Kang, J. Liu, L. Fang, M. Zhou, Optimizing edges and defects of supported MoS_2 catalysts for hydrogen evolution via an external electric field, PCCP. 20 (2018) 26083–26090, https://doi.org/10.1039/c8cp03407a.
[53] C. Jiang, S.L. Rumyantsev, R. Samnakay, M.S. Shur, A.A. Balandin, High-temperature performance of MoS_2 thin-film transistors: Direct current and pulse current-voltage characteristics, J. Appl. Phys. 117 (2015) 064301, , https://doi.org/10.1063/1.4906496.
[54] Y. Yang, Y. Liu, B. Man, M. Zhao, W. Li, Tuning the electronic and magnetic properties of MoS_2 nanotubes with vacancy defects, RSC Adv. 9 (2019) 17203–17210, https://doi.org/10.1039/c8ra08981g.